10 Mrpm Spinning Ball Motor

Preparing the next generation of ultra-high speed drive systems

C. Wildmann, T. Nussbaumer*, J. W. Kolar
ETH Zurich, Power Electronics Systems Laboratory, 8092 Zürich, (Switzerland)
* Levitronix GmbH, 8005 Zürich, (Switzerland)

***Abstract*—This paper presents conceptual ideas for an ultra-high speed spinning ball motor with a target speed in the range of several tens of million rotations per minute. The research should prepare the next generation of ultra-high speed motors. The focus of this work is to investigate physical limitations and discuss feasible concepts for the realization of such drive systems. One major issue is the analysis of the mechanical stresses occurring in the rotor during centrifugal rotation with focus on the rotor shape by using 3D FEM simulation tools. Furthermore, magnetic levitation concepts for a friction-less bearing system are presented and discussed. Two alternative concepts for the position sensing system, which is necessary for detecting the rotor position for the magnetic bearing, are presented and compared. Finally, a first motor prototype is presented to offer basic behavioral insights into the system and its stability.**

***Index Terms*— ultra-high speed drive, spinning ball, asynchronous machine, magnetic bearing.**

I. Introduction

The very high rotational speeds of small motors along with the miniaturization of electrical equipment, makes them of increasing interest. Wherever a compact, accurate, and light-weight solution is sought, e.g. for gyroscopes, centrifuges, drilling devices and in the area of material examination techniques of equipment, these systems have potential for use.

There has been considerable activity in this field of research during recent years. Fig. 1 shows several high-speed systems with respect to their power range which have been realized. A first 1 million rpm / 100 W spindle drive (cf. Fig. 2) was developed recently at the ETH Zurich [1]. This was a first break-through into the million rpm speed drives and has opened up a whole new range of possible applications.

However, for the utilized technology (ceramic ball bearings, permanent magnet rotor, spindle size), the mechanical, thermal and electromagnetic limitations will not allow significantly higher rotation speeds. A ball-type motor in vacuum [2] recently reached 2.88 million rpm. This paper presents concepts for achieving an ultra-high speed drive system in the range of 10 million rpm and more, and investigates effects and limitations on the way there.

As one main obstacle for the achieving these ultra-high rotation speeds is friction, contactless magnetic bearing concepts will be investigated in this paper. A vacuum hose can be employed with these, reducing the air friction losses to nearly zero. As for the second challenge, the inner centrifugal stresses, the paper presents considerations as to how to reduce them by appropriate selection of rotor shape, size, and material. In any case, the rotor must be ferromagnetic in order to be able to levitate it, and as the rotor has to be very small to keep centrifugal stresses low it must be made out of one piece of material. These conditions lead to the asynchronous motor as preferred electrical machine concept [3], where induced surface eddy currents generate the drive torque in combination with the impressed stator field.

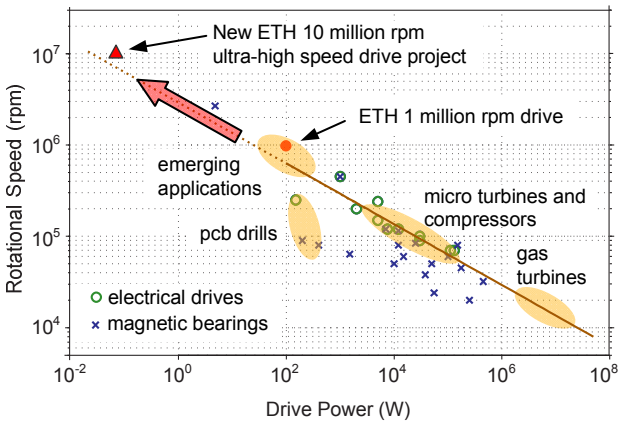

Fig.1 Trends and application areas for ultra-high speed drive systems.

This paper contains considerations and discussions relevant for the realization of such a multi-million spinning ball motor, covering the areas of the magnetic bearing system (section II), the drive concept (section III), the ideal rotor shape based on the analysis of the mechanical stress of the rotor (section IV), and the position sensor system (section V). A prototype system (section VI) will prove the basic functionality.

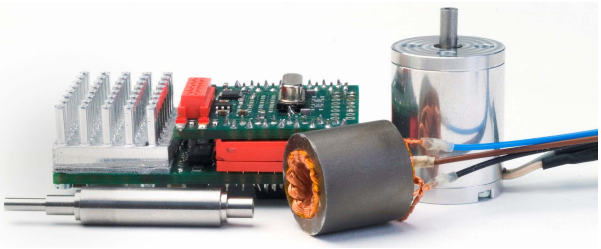

Fig. 2 Realization of a 1'000'000rpm / 100W high speed drive system developed at the ETH Zurich [1] including motor and electronics.

II. Bearing Concepts

Several configurations are possible for the magnetic bearing of a small rotor made out of ferromagnetic material.. The advantages and drawbacks of the various concepts are briefly summarized below.

The rotor spins around the *z*-axis, also referred to as the vertical axis. The radial position describes the location of the rotor in the *xy*-plane. The rotor is modeled as a sphere for the sake of convenience. Other rotor geometries will be investigated in section IV. By using magnets on the drive core, as shown in Fig. 3, the *z*-position of the rotor is passively stabilized. A bearing system needs to be integrated into the drive coils to control the *x*- and *y*-position actively as the rotor is unstable for this configuration in these axes. The advantage of this setup is that disc-shaped rotors as well as spherical rotors can be levitated without any further adaption of its geometry. Long cylinders in *z*-direction on the other hand are unsuitable for this configuration due to their tilting tendencies [4].

If damping in the *z*-direction proves necessary to keep the rotor stable, additional software adjustments have to be made to be able to control the stiffness of the bearing. This may be done by feeding all drive coils with an additional current in the same direction.

Fig. 4 shows a way of keeping the rotor in the center by controlling only the *z*-position. The peak of the bearing core defines the preferred location in *xy*-plane.

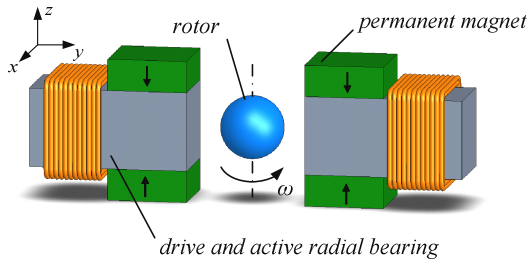

Fig. 3. Configuration using magnets to passively stabilize the rotor in vertical (*z*-) direction and actively control the radial (*xy*-plane) position (bearing and drive units in x-direction are not shown).

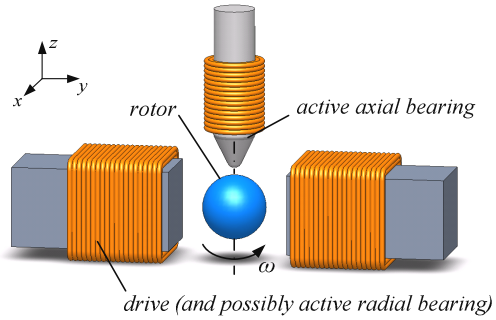

Fig. 4. Configuration using the peak of the bearing core to passively stabilize the rotor in the radial *xy*-plane and actively control the vertical (z-) position (bearing and drive units in x-direction are not shown).

Bearing currents can be superposed with the drive currents in the drive coils with advantage in order to actively damp radial oscillations, which might occur in this setup due to the lack of passive radial damping. Rotors with a long cylindrical shape in the *z*-direction can be levitated, however disc-shaped rotors need an adjustment in their geometry (as e.g. bump, see Fig. 8 (d)) to make levitation possible.

A slight variation of the configuration described above is shown in Fig. 5. This setup requires the control of the rotor position in all directions, as the center position is not a favored position. Any rotor shape can be levitated, but an additional effort has to be put into the software to allow the integration of the bearing into the driving coils (superposed current). All the damping of rotor vibrations has to be active.

To make passive damping possible, a ferromagnetic damping needle can be integrated into the setup as shown in Fig. 6. The preferred position of the rotor is then defined by the upper end of the needle due to the field concentration above it. The needle has to be slightly moveable in the radial directions, but has to be damped mechanically or electrically at the bottom. Nonetheless, all three degrees of freedom can be controlled separately. In addition, any rotor shape can be levitated using this configuration. In order to make the damping needle work properly, the lower part of the rotor must be round-shaped.

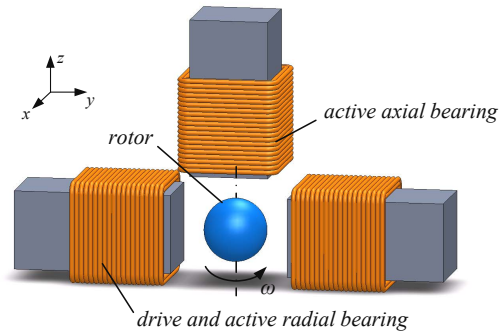

Fig. 5. Configuration to control all degrees of freedom by active bearing units (bearing and drive units in x-direction are not shown).

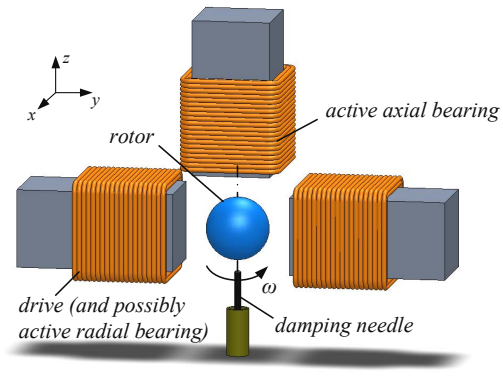

Fig. 6. Configuration to control all degrees of freedom plus introducing passive damping by using a damping needle. Eventually, radial bearings may be omitted (bearing and drive units in x-direction are not shown)

TABLE I. DEPENDENCY OF THE MAXIMAL STRESS OCCURRING IN THE ROTOR DURING HIGH SPEED ROTATION ON THE ROTOR GEOMETRY (n = 25 million rpm, δ = 7850kg/m^3). THE SPHERICAL (BALL-TYPE) SHAPE IS INDICATED IN BOLDFACE.

l [mm]	l/d	$\sigma_{vM,max}$ [GPa]		
		Cylinder shapes		*Ellipsoid shapes* with 2nd order spline profile
		No chamfered edges (r_A = 0)	*Chamfered edges* with r_A = min(l/2;d/2)	
0.04	0.05	3.531	3.458	3.231
0.15	0.1875	3.556	3.291	2.348
0.2	0.25	3.579	3.227	2.587
0.4	0.5	3.655	3.290	3.273
0.8	1	3.384	**3.649 (ball-type)**	2.956
1.6	2	3.347	3.277	3.116
4	5	3.353	3.277	3.018

III. DRIVE CONCEPT

The utilized drive concept is an asynchronous machine type. A rotary field is applied on the rotor while it is being levitated. Due to the changing flux through the rotor eddy currents occur on the surface of it. These currents and the applied rotary magnetic field produce torque acting on the rotor. The torque generated this way accelerates the rotor to a speed near to the rotary speed of the rotary magnetic field, where the friction losses and the input power become even.

IV. STRESS ANALYSIS OF THE ROTOR

The maximal stress $\sigma_{vM,max}$ occurring in the center of the rotor can be calculated as

$$\sigma_{vM,max} = K \cdot \rho \cdot \left(\frac{d}{2}\right)^2 \cdot \omega^2 , \qquad (1)$$

where K is a shape factor describing the dependency of the occurring stresses on the geometry of the rotor, ρ is the density of the rotor material, d is the diameter of the rotor and ω is the rotational speed in rad/s [2].

According to this formula the material as well as the shape of the rotor influences the maximal rotational speed. In order to prevent the explosion of the rotor, the maximal stress of the rotor $\sigma_{vM,max}$ has to be smaller than the yield strength of the rotor material. The goal of the stress analysis is to reveal how to reduce the maximal occurring rotor stress $\sigma_{vM,max}$ by adjusting the geometry of the rotor, in other words, finding a physically reasonable shape with the smallest possible shape factor K. The selection of the material is treated subsequently.

The following points apply for simulations calculating the centrifugal forces of the rotor, unless specified otherwise:

- Hook's law is also valid above the limit of elasticity: The stress-strain curve of the material is linear so the load limit of the material is disregarded. Thus, a stress value is determined which the material in reality only may bear if it is below the yield strength. A stress value above the yield strength leads to hardware failure.
- Material density: ρ = 7850 kg/m^3 (steel)
- Target revolution speed: n = 25 million rpm
- Diameter: d = 0.8 mm

The mechanical stress distribution occurring in a spherical rotor is shown in Fig. 7 with the parameter described above. The stress distribution is calculated using 3D FEM analysis in *SolidWorks*™. As can be seen in Fig. 7, the maximum stress occurs in the ball center and decreases to approximately 1/3 of the maximum value towards the radial direction, while the stress drops off to nearly zero towards the axial direction.

This already gives an indication that with geometrical variations an improvement is probably possible. Thus, various different rotor geometries have been analyzed

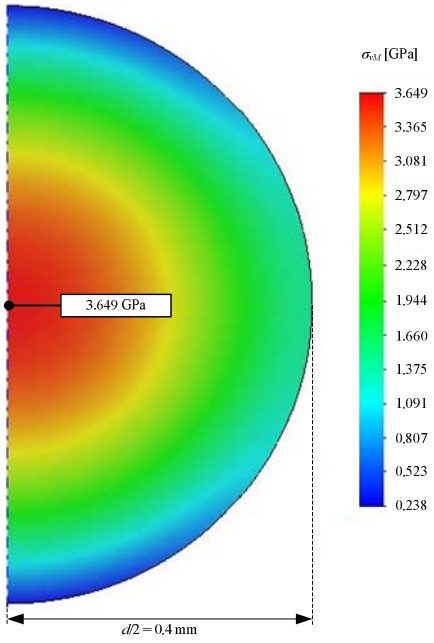

Fig. 7. Stress distribution in a spherical rotor (d = 0.8mm, n = 25 million rpm, δ = 7850kg/m^3).

regarding their occurring mechanical stresses at the specified target revolution speed, whereby the following geometrical parameters have been used:

- l: length of the rotor in z-direction (i.e. the height)
- d: rotor diameter
- r_A: radius used to chamfer the edges, whereby $r_A = \min(l/2;d/2)$ is used exemplarily.

Table I shows the centrifugal stresses $\sigma_{vM,max}$ calculated for different rotor geometries for a constant rotor diameter $d = 0.8$ mm and different rotor heights l. Some selected examples are shown in Fig. 8. The results will be discussed below.

It seems that high cylinders ($l/d > 1$) are generally more advantageous than disc-shaped rotors (with $l/d < 1$). for the basic cylindrical rotor forms (without any chamfering of the edges), Especially, $l/d = 0.5$ proves to be a very disadvantageous selection.

The situation changes, if the rotor edges are chamfered with $r_A = \min(l/2;d/2)$, which results in rotor shapes as shown in Fig. 8(a) and (b). The best form here is a disc-shaped rotor with $l/d = 0.25$, where the maximum occurring stress is reduced by about 10%, while the high

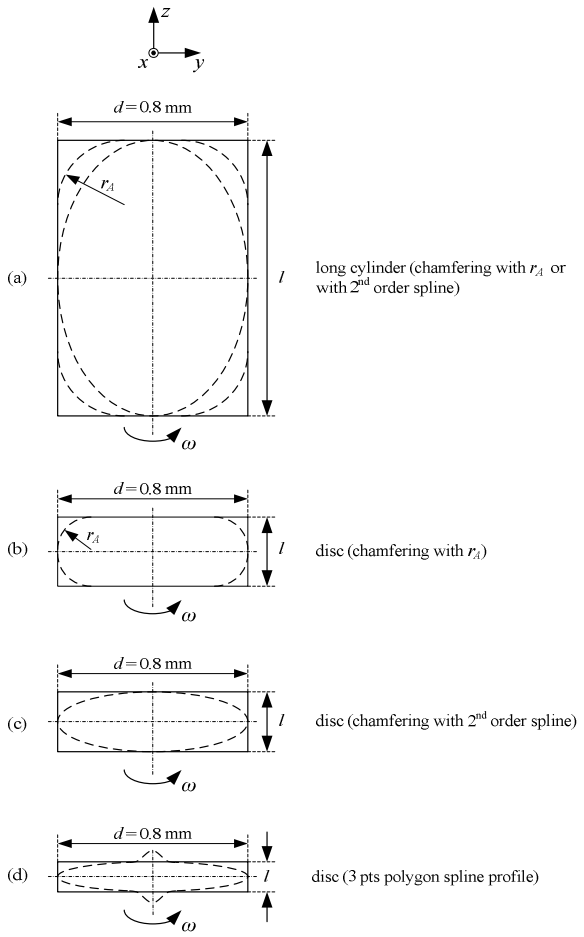

Fig. 8. Rotor profiles used in simulations for calculating centrifugal stresses.

TABLE II. MAXIMAL REVOLUTION SPEED n_{max} FOR DIFFERENT ROTOR MATERIAL AND ROTOR SHAPE ($d = 0.8$ mm).

Material	Density ρ [kg/m^3]	Yield strength σ_Y [GPa]	Maximal revolution speed n_{max} [million rpm]	
			Spherical rotor	Disc rotor (2nd order spline)
AISI 440C (steel)	7850	1.9	18.0	22.5
Metallic glass	7800	5	29.4	36.6
Carbon nanotubes	1400	10	98.0	122.2

cylindrical shapes are not improved significantly by chamfering. Rounding off the edges of a cylinder with $l/d = 1$ surprisingly, even has a negative impact. The centrifugal stress is increased by about 8% for this shape, which is then identical to a spherical (ball-shaped) rotor, and results in the aforementioned value ($\sigma_{vM,max} = 3.649$ GPa, cf. Fig. 7).

If splines are used to chamfer the edges [cf. Fig. 8(a) and (c)] the maximal stress can be reduced by an even greater extent throughout all rotor geometries, e.g., for a 2nd order spline a disc-shaped rotor with $l/d = 0.1875$ the reduction of the maximal stress with respect to the original disc shape is 34%.

Thus, by carefully choosing the rotor profile the maximum stresses occurring in the rotor can be substantially reduced. It must also be considered that disc-shaped rotors ($l/d < 1$) are more suitable for high speed rotation than high cylinders ($l/d > 1$) due to the danger of bending high cylindrical shapes at high rotational speeds [4].

Taking all these considerations into account, a disc-shaped rotor with appropriate shaping of the edges is most preferable from the viewpoint of mechanical stability, but requires a rotor shape adaption at the top [i.e. a bump as shown in Fig. 8(d)] in order to make stable levitation feasible for some bearing concepts.

A spherical rotor, on the other hand, has clear advantages concerning the mechanical fabrication process as well as the magnetic bearing properties. However, it is characterized by clearly higher centrifugal stresses.

Table II shows the maximum achievable revolution speed n_{max} with different rotor material and shapes for a given rotor diameter $d = 0.8$ mm. Unfortunately, not every material is suited for magnetic bearings, as it must be ferromagnetic. This is why carbon nanotubes are out of the question. In addition, precise geometry is required. Metallic glass has to be cooled down quickly during the production process (from 10^{-1} K/s until 10^{7} K/s [4]) to maintain its amorphous structure, which makes – at least at the moment – precise material forming impossible. Common steel seems to be the best choice. Spherical rotors used for mechanical bearings can be purchased commercially down to the size of half a millimeter.

V. Sensor Concepts

Especially two sensor types are convenient to determine the rotor position in the setup of the high speed motor, namely eddy current sensors and optical laser sensors. The advantages are in their high precision and fast response time (high bandwidth) and the fact that they are unlikely to interfere with environmental conditions such as the temperature, pressure and leakage fields.

Eddy current sensors can be used in an arrangement below the rotor, as shown in Fig. 9. By adding the signals of all four coils the z-position is calculated. By looking at the difference of the signals of two oppositely placed sensor coils the x- and y-position of the rotor can be determined. If only the z-position is needed to keep the rotor in place, one sensor coil directly beneath the rotor is sufficient.

An advantage of eddy current sensors is that they can measure through any non-conductive material. This can be of significance, if the rotor is encapsulated from the rest of the motor in a vacuum hose. Its resolution, however, is extremely dependent on the distance between the rotor and the sensor coils. In addition, in order to detect the rotor position fast enough to make active damping possible, the excitation frequency of the coils must be at least twice as high as the rotational speed, which is a consequence of the sampling theorem. In practice, the excitation frequency is preferably chosen at least ten times higher than the rotational speed. The skin effect and the parasitic capacitance of the excitation coils at high frequencies limit the excitation frequency to about 10 MHz.

By using laser modules and photosensitive quadrant diodes the rotor position can also be determined. Fig. 10 shows the principle of how the measurement works. A laser beam is aimed at the rotor, while the projection of its shadow is detected on a quadrant photodiode. By calculating the difference of the signals coming from opposing surfaces of the quadrant diode the x-, y- and z-position of the rotor can be determined. A maximum of two degrees of freedom (in Fig. 10 x- and z-position) can be measured for one pair of a laser module and a photodiode, as the projection of the shadow only moves if the rotor is moving perpendicularly to the laser beam. Between the rotor position and the four signals A, B, C and D following relation applies:

$$x \propto B + C - (A + D) \tag{2}$$

$$z \propto A + B - (C + D) \tag{3}$$

The y-position can be determined in a similar way with the use of a second pair of laser module and quadrant photodiode positioned perpendicularly to the one shown in Fig. 10.

The rotor has to be visible to the laser module and the diode to be able to use this sensor type The advantage

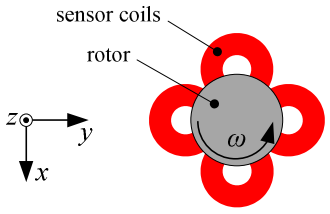

Fig. 9. Arrangement of four eddy current sensor coils underneath the rotor to determine the rotor position in all directions.

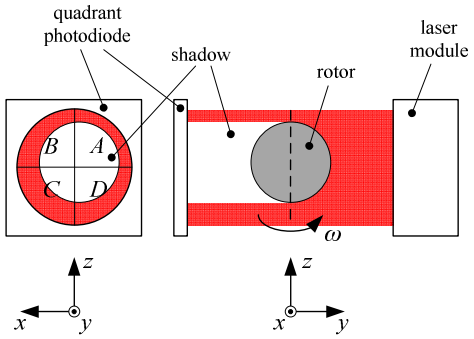

Fig. 10. Measurement principle of the optical sensor composed of a laser module and a quadrant photodiode.

of optical sensors is that they do not to interfere at all with the electromagnetic field originating from the motor drive.

VI. Experimental Test Setup

In order to verify the aforementioned considerations a first prototype system has been designed and built. The objective of this system is to investigate basic magnetic bearing properties, the sensor system, the effect of high-order harmonics originating from the drive coils on the rotor stability and the effect of passive and active damping on radial rotor vibrations without miniaturization issues. Thus, the whole system has been enlarged. As rotor diameter of 4 mm instead of 0.8 mm has been chosen. Very large stator system and air gap clearance have been chosen in order to allow the testing of various sensor configurations. As a 3D FEM analysis using the *Maxwell 3D*™ simulation tool revealed, the large clearances cause a nearly perfectly sinusoidal field distribution (with sinusoidal current feed of the drive coils), which allows the analysis of the effect of higher harmonics of the drive system on the rotor stability. Obviously, this design is a preliminary one, which only allows rotation speeds in the range of 100'000 rpm.

In the following, the specifications and considerations for the first prototype are listed:

- The drive core dimensions are: $h_s = 8$ mm, $w_s = 9$ mm and $\delta = 10$ mm (cf. Fig. 11).
- The rotor diameter is chosen to be 4 mm. However, the setup also allows levitating and rotating smaller rotors.
- Air gap δ_b: The air gap between the rotor and the

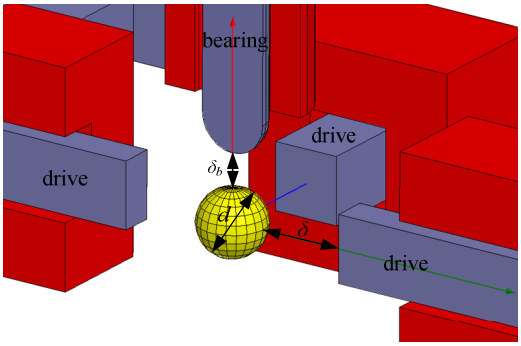

Fig. 11. Parameters describing the configuration of the prototype.

bearing core δ_b can be continuously varied from 0.3 mm up to about 10 mm.

- Optical and eddy current sensors: The architecture allows the integration of both optical sensors as well as small eddy current sensors (four sensor coils arranged in a circle or a sensor coil in the center below the rotor).
- Damping mechanism: Under the rotor cap there is enough space for the integration an additional stabilization and damping mechanism (needle in fluid or the like).
- Encapsulation of the rotor: The possibility of encapsulation provides additional protection against flying particles of the rotor. It also reduces the sensitivity of the photodiodes to the outside world.

Fig. 12 shows the prototype with the rotor (d = 4 mm) being levitated. Fig. 13 shows magnetic bearing and drive currents at a rotation speed of 60'000 rpm. The rotor speed was determined by measuring reflections of the rotor which was possible due coloring one half of the surface with a conventional marker (cf. Fig. 12).

The experiments have shown that the rotor can be passively stabilized very well in the *xy*-plane by using a damping needle placed underneath the rotor. Furthermore, high-order harmonics above 100 Hz do not excite any rotor instability. This relates to the fact that for a future design the creation of a purely sinusoidal magnetic field is not a requirement.

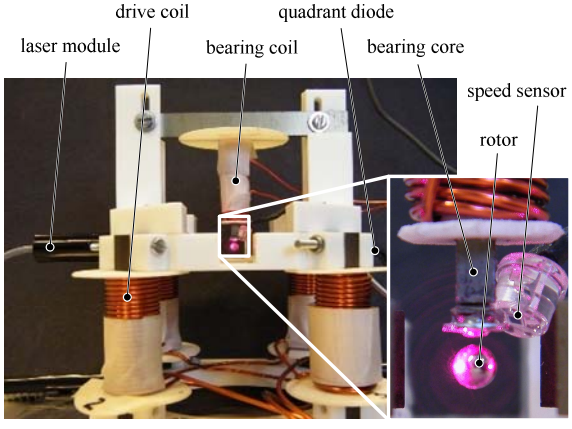

Fig. 12. Prototype of the high speed motor (d = 4 mm).

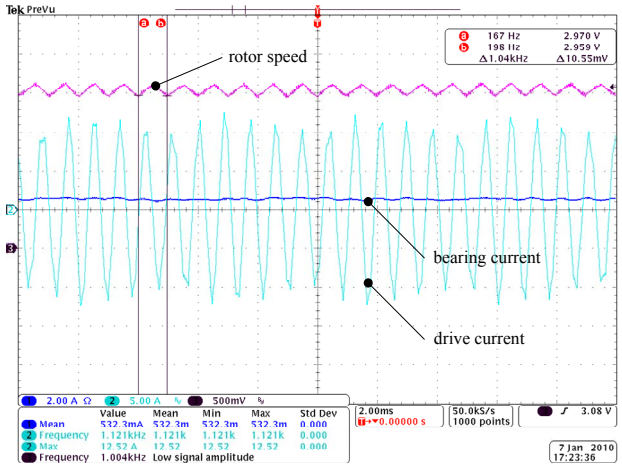

Fig. 13. Drive and bearing currents for a rotor (d = 4 mm, with passive damping by damping needle) stably spinning at 60'000 rpm.

The investigation also showed that iron losses become considerable already at comparable low frequencies. At a rotary field of 1.5 kHz and a magnetic field density in the drive cores of 1 T the temperature reaches 50°C (switching frequency: 35 kHz). Therefore, in a future design the possibility of iron-less drive cores should be evaluated carefully. Both sensor systems worked satisfactory for the position detection, however, the optical sensors were preferred due to their better signal quality independently of the electromagnetic environment and their better handling.

VII. Outlook

Based on these experiences, a future design can already directly target the ultra-high speeds in the range of several millions of rpm. This requires a re-design of the drive system (possibly without iron material), a significantly smaller motor construction, which, however, still allows the integration of a vacuum hose. These tasks will be performed in the course of research and will be reported in a future publication.

References

[1] C. Zwyssig, J.W. Kolar, S.D. Round, "Megaspeed Drive Systems: Pushing Beyond 1 Million r/min," *IEEE/ASME Trans. Mechatron.,* vol. 14, no. 5, pp. 564-574, Oct. 2009.

[2] A.R. Boletis, "High Speed Micromotor on a Three Axis Active Magnetic Bearing", *École Polytechnique Fédérale de Lausanne*, Ph. Diss. No. 3160, 2005.

[3] J.W. Beams, J.L. Young III, J.W. Moore "The Production of High Centrifugal Fields", *Journal of Applied Physics*, vol. 17, no. 5, pp. 886–890, 1946.

[4] L.E. MacHattie, "The Production of High Rotational Speed", *Review of Scientific Instruments*, vol. 12 p. 429, 1941.

[5] A. Inoue, Stabilization of metallic supercooled liquid and bulk amorphous alloys", *Acta materialia,* vol. 48, no. 1, pp. 279–306, 2000.

[6] A. Inoue, B.L. Shen, H. Koshiba, H. Kato, A.R. Yavari, "Ultra-high strength above 5000 MPa and soft magnetic properties of Co–Fe–Ta–B bulk glassy alloys", *Acta Materialia*, vol. 52, no. 6, pp. 1631–1637, 2004.